An ab Initio QCISD Study of the Potential Energy Surface for the Reaction HNO + NO → N_2O + OH

Steven W. Bunte, Betsy M. Rice, and Cary F. Chabalowski*

U.S. Army Research Laboratory, AMSRL-WM-PC, Aberdeen Proving Ground, Maryland 21005-5066

Received: May 28, 1997; In Final Form: August 13, 1997[⊗]

Results are presented from ab initio quantum chemical calculations on the ground-state potential energy surface for the open shell doublet reaction: HNO + NO → N_2O + OH (reaction I). This reaction is thought to be important in the sustained combustion of nitrogen-containing fuels. Geometry optimizations have been carried out at the QCISD/6-31G(d,p) level using unrestricted Hartree−Fock zeroth-order wave functions in search of local minima and transition states, followed by energy refinements for all critical points at the QCISD(T)/6-311+G(2df,2p) level. All saddle points were subjected to intrinsic reaction coordinate calculations to determine the minima to which they connect. We report two completed reaction pathways for reaction I. Some of these results will be compared with earlier work by others on the same reaction where geometry optimizations were carried out primarily at the UMP2/6-311G(d,p) level. The comparison brings to light some interesting differences between QCISD and UMP2 theories in the prediction of molecular structures and the connectivity of critical points (and therefore, connected reaction paths) for the doublet system in reaction I.

I. Introduction

Chemical reactions involving HNO and NO are considered to be key processes in the combustion of nitrogen-containing fuels. Our primary interest in NO chemistry centers upon its role in controlling ignition chemistry in the dark zone of nitramine-based gun propellants. One of the distinctive features observed during the combustion of nitramine-containing solid propellants is the two-stage nature of the flame. At pressures of ∼2 MPa, there is a separation between the solid surface and the gas-phase luminous flame that is typically 0.5 cm wide. This nonluminous region is commonly referred to as the dark zone. The dark zone is believed to contain NO and NO-containing intermediates that react slowly. Detailed kinetic modeling of the dark zone coupled with a sensitivity analysis of the reaction set used in the model by Vanderhoff and co-workers[1] indicate that the reaction

$$\mathrm{HNO + NO \rightarrow N_2O + OH} \qquad \text{(I)}$$

is the most sensitive in controlling the ignition chemistry of nitramine propellants. This reaction is the rate-controlling step in the thermal reduction of NO by H_2 at temperatures greater than 1000 K. In addition, this reaction is also known to initiate the formation of N_2 and H_2O.[2,3]

There have been theoretical studies of related reactions involving hydrogen and NO, where some of the more recent work includes the reactions HNO + H,[4,5] HNO + OH,[6] and NH + NO_2.[7] To date, there has been no direct experimental measurement of the rate for the HNO + NO reaction, presumably due to the difficulties associated with making HNO. The rate constant, however, has been estimated by Wilde[8] to be $10^{12.3+0.3}$ exp(−260000 ± 5000/*RT*) cm^3/(mol s) over the temperature range 800−1060 °C. This estimate was obtained from kinetic modeling by Graven[9] and from measurements for the rate of NO disappearance by Kaufman and Decker[10] and pressure changes by Hinshelwood et al.,[11,12] all of whom were studying the kinetics of the H_2 + NO system.

In light of the suggestion that reaction I is perhaps the rate-controlling step in the chemistry of the dark zone of a nitramine propellant flame, we initiated an ab initio study of the reaction of HNO + NO. During the preliminary stages of our calculations, Mebel, Morokuma, Lin, and Melius[13] (MMLM) published many critical points for the HNO + NO potential energy surface (PES) and information about the reaction paths leading to products. All of these critical points were described at the UQCISD(T)/6-311G(d,p)//UMP2/6-311G(d,p) level. Energies of the critical points on their "minimum energy reaction path (MERP)"[13] were refined using a modified version of the Gaussian-2 (G2)[14] scheme (referred to as G2(PU)). In their G2-(PU) approach, UMP2/6-311G(d,p)[15] (i.e., projected UHF-MP2[15]) is used to optimize all geometries (with two exceptions). The geometries of reactants and the transition state corresponding to the rate-determining step were optimized at the UQCISD/6-311G(d,p) level and used in the G2(PU) scheme. The results of their study suggest that the rate determining barrier for reaction I is a 1,3-hydrogen migration with a barrier height of 21.6 kcal/mol. In an earlier study Mebel, Morokuma, and Lin[7] used UMP2 theory to predict structures on the PES of a related reaction where NH + NO_2 proceeds to two products, namely HNO + NO and N_2O + OH, which are the reactants and products of reaction I, respectively.

Our early results on this system led us to believe that UMP2 is not capable of adequately describing the electronic structure in this system. This conclusion is based on the fact that many points on the PES of reaction I have UHF zeroth-order wave functions with large spin contamination, where some S^2 values are as large as 1.36 (the correct value is 0.75). It is well-known that open shell molecules described by unrestricted Hartree−Fock (UHF) orbitals are subject to such spin contamination. This has been cited as one possible cause for the slow convergence in the MP series.[16−19] In choosing a more suitable (yet computationally feasible) approach, we decided to locate critical points on portions of the PES at the QCISD level. Studies have shown that coupled cluster theory, of which QCISD is a subset, is effective in correcting for spin contamination[20] in the UHF wave function, and QCISD has been shown to

[⊗] Abstract published in *Advance ACS Abstracts,* November 15, 1997.

S1089-5639(97)01716-7 CCC: $14.00

predict relative energies in good agreement with experiment for another doublet system.[21] As further justification for the use of these methods in predicting relative energies on an open shell system, we cite the work of Lee et al.[22] on Be and Mg clusters. Lee et al.[22] have shown that relative energies, in the form of binding energies, calculated at the CCSD(T) and QCISD(T) levels for small Be and Mg clusters reproduce "...the accurate MRCI values very well." These are clusters with electronic states purported to be of multireference character.[22] This implies that the approximate inclusion of triples in CCSD(T) and QCISD(T) provides some of the important correlation corrections obtained in a multireference treatment. For the above reasons, all critical points on the PES have been optimized at the UQCISD/6-31G(d,p) level, followed by energy refinement at the UQCISD(T)/6-311+G(2df,2p) level. Basis set dependence has been investigated by optimizing several critical points on the PES at the UQCISD level using a triple-ζ basis set.

Most of the critical points described in this work are features of two completed reaction paths for reaction I. These paths were established through intrinsic reaction coordinate (IRC) calculations leading from the various transition states to local minima. While we make no claim to having found all possible pathways for reaction I, the results presented here offer a convincing argument that the two paths determined in this study are continuously connected from reactants to products. The minimum energy pathway reported here differs from that reported by MMLM. These differences in features along the reaction paths could lead to different conclusions regarding mechanisms for reaction I. Significant inconsistencies are noted between a number of the UQCISD structures from this study and the UMP2 structures from previous works.[7,13]

II. Methods

All calculations describing the PES were performed using the Gaussian 92[30a] (G92) or Gaussian 94[30b] (G94) set of computer codes. Critical points on the PES were determined through UQCISD[23]/6-31G(d,p)[24] geometry optimizations (using a frozen core), where gradients were converged to at least the default settings. Henceforth, it will be understood that all zeroth-order wave functions are of the UHF type, and the "U" label will be dropped from the correlation treatment designation. Each critical point was characterized through normal-mode analysis. In addition, a stability check[25] (with default perturbations) was run on the UHF wave functions. All transition states reported here had one imaginary frequency, and all minima had no imaginary frequencies. The transition states were subjected to IRC[26] calculations (using the default step size) to facilitate connection with minima along the reaction paths. Each IRC terminated upon reaching a minimum as defined by the default criteria provided in G92 or G94, unless otherwise stated. For those points that did not terminate in this fashion, the last converged point on the reaction path was used as the initial structure for a full geometry optimization. For each instance in which such an optimization was attempted, a local minimum was found. It is assumed that this is the minimum to which the IRC would have walked if convergence problems had not been encountered. Energies and geometries will be given to justify the conclusion that the IRC was proceeding to the same minimum located by the subsequent optimization. Once all critical points for the reaction paths were determined, the energies were refined (using a frozen core) at the QCISD(T)[23a]/6-311+G(2df,2p)[27−29]//QCISD/6-31G(d,p) level. These refined energies were then corrected for zero-point energies using the QCISD/6-31G(d,p) structures and frequencies.

Some critical points on the PES have spin S^2 values substantially above the 0.75 magnitude expected for a doublet system. The proper way to assess the capability of the QCISD method for correcting this spin contamination in the UHF wave function is to calculate the S^2 expectation value over the QCISD density. Unfortunately, we do not have access to codes that include this capability. We can, however, calculate this expectation value for the coupled-cluster singles and doubles[31,32,33] (CCSD) method (with no frozen orbitals) using our version of the ACES II quantum chemistry package[34] which includes the code for $\langle S^2 \rangle_{CC}$ written by Stanton.[20] Even though QCISD is only a subset of the full representation of the CCSD equations,[22,33,35−37] it will be assumed that the two approaches give similar expectation values of S^2.

III. Results and Discussion

Absolute, relative, and zero-point energies, and S^2 values of the critical points on the HNO + NO PES are given in Table 1. Harmonic vibrational frequencies of all critical points calculated at the QCISD/6-31G(d,p) level are given in supplementary Table 1S. We have calculated the CCSD S^2 expectation values for five selected critical points on the PES where the UHF S^2 is large. From Table 1 we see that the S^2's before and after the CCSD calculations are **A**(1.36 → 0.81); **E**(1.28 → 0.77); **F**(1.36 → 0.82); **L**(1.28 → 0.77); **N**(1.11 → 0.76). The most heavily contaminated UHF wave function has its spin corrected to 0.82, where the correct value is 0.75 for a doublet system.

It has been shown that QCISD neglects certain terms in the energy expression produced by the single excitation operator T_1 that are present in the complete CCSD treatment.[22,33,35−37] Therefore, QCISD could produce significantly different relative energies along the reaction paths than CCSD, which would cast doubt upon the ability of QCISD to achieve the primary goal of this study, which is to accurately map the relative energetics defining the PES. Lee et al.[22] concluded from their study of 18 different chemical species that "...the better the SCF wave function approximates the true wave function, the better the agreement between the QCISD and CCSD correlation energies." To ascertain the impact on the relative energies due to neglecting the T_1-containing terms, CCSD[34]/6-31G(d,p) calculations were performed on the five points mentioned above with the worst UHF S^2 values. Table 2 contains the energies of each of the five structures relative to the reactants for QCISD versus CCSD. This table also contains the absolute total energies at each point for both QCISD and CCSD methods, and the difference between the absolute QCISD and CCSD energies at each point. All calculations were done with frozen core orbitals to be consistent with our geometry optimizations. The geometries and zero-point energy corrections were taken from the QCISD/6-31G(d,p) calculations. There are several points worth noting concerning Table 2. As pointed out by Lee et al.,[22] QCISD tends to overestimate the correlation correction and hence produces absolute energies lower than those of CCSD. This trend is again seen in the data of Table 2. The first important point to note is that the difference between the QCISD and CCSD absolute energies for each structure "*i*", defined as $\Delta E_i^{abs} = E_i(\text{QCISD}) - E_i(\text{CCSD})$, is nearly constant over the five points (**A**, **E**, **F**, **L**, **N**) on the PES, falling in the range 0.00484−0.00528 hartrees, or 3.04−3.31 kcal/mol. The second important point is that the difference in QCISD versus CCSD energies for the reactants is 2.59 kcal/mol. For the five structures on the PES, this produces a maximum and average difference in relative energies between CCSD and QCISD of 0.72 and 0.56 kcal/mol, respectively. The largest difference belongs to structure **F**, which also has the worst UHF S^2 value. On the basis of this data it is assumed that the QCISD PES for this

TABLE 1: Absolute Energies, Zero-Point Energies (ZPE), Zero-Point Corrected Relative Energies, and S^2 Values for Species on the HNO + NO Potential Energy Surface. All Geometries Optimized at QCISD/6-31G(d,p)

					CCSD[d]	QCISD/6-31G(d,p)			QCISD(T)/6-311+G(2df,2p)	
species	type	symmetry[a]	S^2, 0[b]	S^2, A[c]	$\langle S^2 \rangle$	ZPE[e]	absolute E[f]	relative E[e,g]	absolute E	relative E[e,g]
HNO + NO	min	(^{1}A′; $^2\Pi$)	0.888	0.753		11.65	−259.716 221	0.00	−260.002 812	0.00
A	TS		1.355	0.922	0.81	13.95	−259.697 014	14.35	−259.993 147	8.37
B	min	^{2}A″	1.054	0.761		15.47	−259.714 782	4.72	−260.010 027	−0.71
C	TS		1.076	0.797		11.27	−259.624 257	57.33	−259.921 806	50.45
C′	TS	^{2}A″	1.055	0.792		11.23	−259.623 894	57.52	−259.923 085	49.61
D	min	^{2}A′	1.074	0.767		15.75	−259.717 231	−3.47	−260.012 869	−2.21
E	TS	^{2}A′	1.277	0.945	0.77	13.93	−259.701 227	11.69	−260.002 676	2.37
F	TS		1.357	0.913	0.82	13.70	−259.692 404	17.00	−259.988 105	11.28
G	min	^{2}A″	1.054	0.760		15.45	−259.716 297	3.75	−260.010 545	−1.05
H	TS	^{2}A″	0.994	0.758		12.61	−259.667 160	31.75	−259.966 148	23.97
I	min	^{2}A″	1.097	0.764		15.12	−259.708 447	8.35	−260.000 958	4.63
J	TS		1.068	0.761		13.67	−259.704 683	9.26	−259.996 262	6.13
K	min	^{2}A′	1.123	0.770		15.48	−259.711 148	7.01	−260.007 998	0.58
L	TS	^{2}A′	1.279	0.951	0.77	13.44	−259.684 616	21.62	−259.986 745	11.87
M	TS		1.018	0.763		14.68	−259.690 147	19.39	−259.986 227	13.44
N′	TS		1.107	0.795	0.76	11.20	−259.621 828	58.78	−259.918 767	52.29
N	TS	^{2}A′	1.216	0.788		11.61	−259.601 492	71.95	−259.899 969	64.50
HO + N_2O	min	($^2\Pi$; $^1\Sigma^+$)	0.755	0.750		11.44	−259.737 825	−13.77	−260.033 766	−19.63

[a] If no symmetry is designated, the point group is C_1. All ^{1,2}A states belong to C_S point group. NO, HO, and N_2O belong to the $C_{\infty v}$ point group. [b] The expectation value of S^2 before projection. [c] The expectation value of S^2 after projection. [d] The CCSD S^2 value is calculated using ACES II[34] via the method of Stanton.[20] [e] Values given in kcal/mol. [f] Values given in hartrees. [g] Includes QCISD/6-31G(d,p) zero-point energy.

TABLE 2: QCISD[a]/6-31G(d,p) versus CCSD/6-31G(d,p) Energies for Selected Structures from the PES with Large S^2 Values (QCISD/6-31G(d,p) Geometries and ZPE Corrections Used for All Structures)

	absolute energy (hartree)	absolute energy (hartree)	ΔE_i^{abs}	ΔE_i^{PES} (kcal/mol)[e]		$\Delta\Delta E^{PES}$
species[b]	E_i(CCSD)[c]	E_i(QCISD)[c]	(kcal/mol)[d]	CCSD	QCISD	(kcal/mol)[f]
HNO	−130.143 503	−130.144 758	0.79			
NO	−129.568 597	−129.571 463	1.80	0.00	0.00	0.00
A	−259.691 897	−259.697 014	3.21	14.98	14.35	0.63
E	−259.696 261	−259.701 227	3.11	12.22	11.69	0.53
F	−259.687 125	−259.692 404	3.31	17.72	17.00	0.72
L	−259.679 774	−259.684 616	3.04	22.07	21.62	0.45
N	−259.616 906	−259.621 828	3.09	59.29	58.78	0.51

[a] Frozen core used in both QCISD and CCSD calculations. [b] See Figures 1, 2, and 3 for structures, and Table 1 for electronic state symmetry. [c] QCISD calculated from Gaussian 92 and 94,[30] and CCSD calculated using ACES II program.[34] Subscript "i" refers to the structure label. [d] $\Delta E_i^{abs} = E_i$(QCISD) − E_i(CCSD). [e] $\Delta E_i^{PES} = E_i - E_{HNO+NO}$, including ZPE from the QCISD(FC)/6-31G(d,p) calculations. See Table 1 for ZPE values. [f] $\Delta\Delta E^{PES} = \Delta E^{PES}$(CCSD) − ΔE^{PES}(QCISD) from previous two columns.

reaction would agree with a complete CCSD PES to within ∼1.0 kcal/mol or less for all structures, which is probably smaller than the error in the ΔE's associated with this level of theory. Hence, no attempt was made to repeat these computationally intensive calculations at the CCSD level for the remaining points on the PES.

Two paths leading to formation of the products of reaction I have been established through IRC calculations from the transition states optimized at the QCISD/6-31G(d,p) level. Figures 1 and 2 show diagrams of relative energies along reaction paths 1 and 2, respectively. The geometries of the stationary points are placed at their appropriate locations along the reaction paths. Each structure is labeled alphabetically in these figures to associate the structure with the species listed in Tables 1 and 2 and in the following discussion. Unless otherwise stated, all barrier heights discussed throughout this paper correspond to the highest level of calculation (QCISD-(T)/6-311+G(2df,2p)//QCISD/6-31G(d,f)) and have been corrected for zero-point energy.

The two reaction pathways are similar in that the first step involves formation of the HN(O)NO intermediate through N−N bond formation, which then undergoes a hydrogen migration as the reaction proceeds. All references to cis or trans conformations are relative to the four heavy atoms unless otherwise noted. Path 1 (Figure 1), whose first step is formation of cis HN(O)NO, proceeds to products through a 1,2-hydrogen migration reaction. Path 2 (Figure 2), proceeds through formation of trans HN(O)NO which subsequently undergoes a 1,3-hydrogen shift. Our results begin to differ from MMLM's immediately after the formation of the entrance channel transition state (TS). In our study, the cis entrance channel barrier **A** in path 1 goes on to form a minimum cis structure **B**. The trans entrance channel TS **F** in path 2 remains trans as it proceeds to the minimum structure **G**. MMLM report a single cis entrance channel transition state, **1′**, that proceeds to a minimum trans structure, **2**. For comparison, the MERP of MMLM has been reconstructed in Figure 3, with the reported structures (including **1′** and **2**) at each critical point. At this point, we will discuss features of reaction paths 1 and 2 separately.

A. Path 1. Critical point **A** is a loose, nonplanar transition state with an N−N distance of 1.90 Å and HNO and NO moieties closely resembling the isolated molecules (see Figure 1). The intermediate formed upon crossing this barrier (structure **B** in Figure 1) is cis planar and has an N−N bond distance of 1.42 Å. IRC calculations for the walk **A** → **B** terminated upon reaching the local minimum **B**. The IRC walk of **A** → reactants terminated when the energy was within 0.43 kcal/mol of the reactant asymptote and the geometric parameters of the species were within 0.2% or less of the reactants' values. Two reaction pathways were found starting from **B**. The lower energy path proceeds over the TS structure representing a simple torsion around the N−N bond. IRCs from this TS, denoted as structure **M** in Figure 1, connect paths 1 and 2 by the relationship **B** → **M** → **G**.

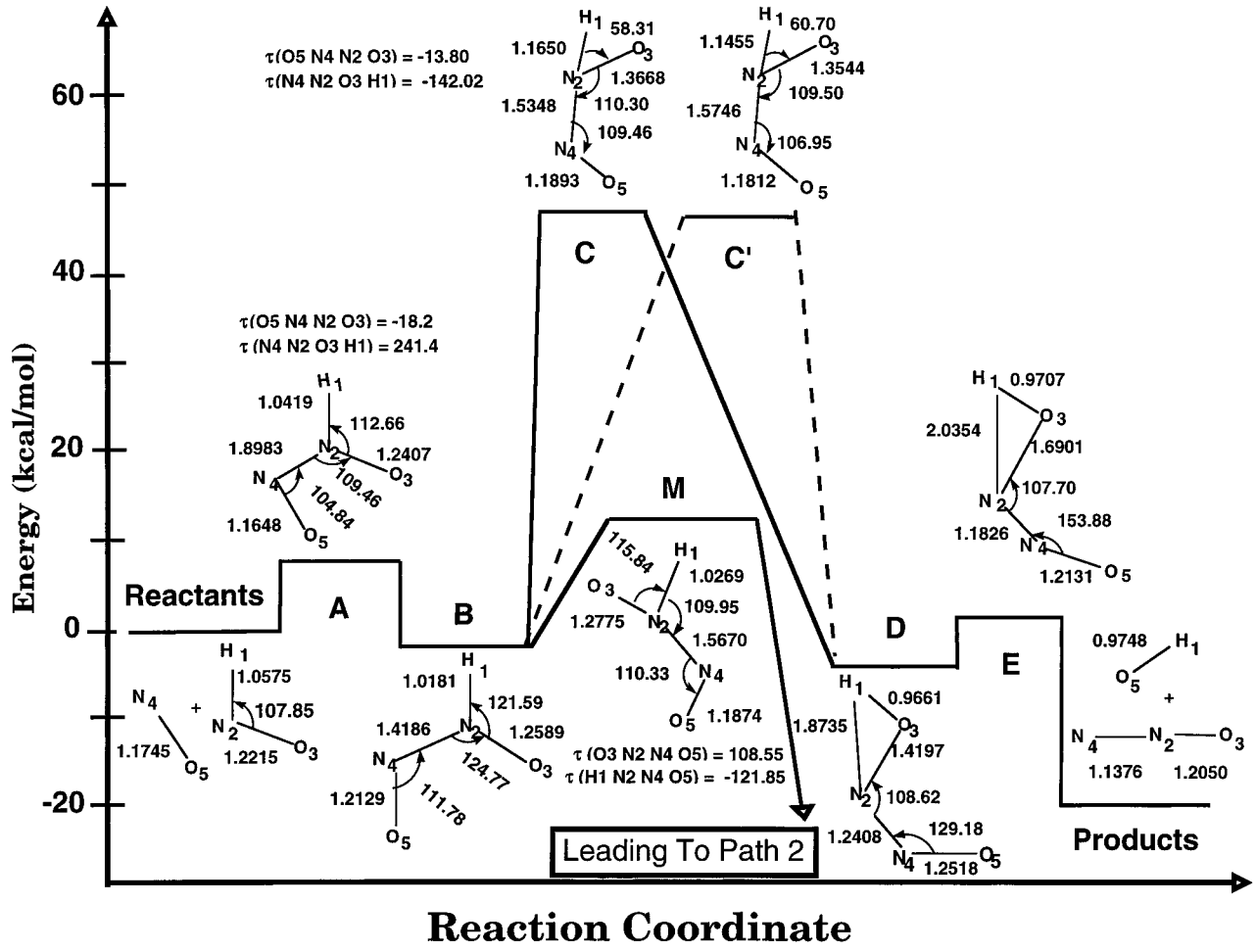

Figure 1. Pathway 1 for reaction I. All structures and relative energies are for zero-point corrected energies calculated at the QCISD/6-311+G-(2df,2p)//QCISD/6-31G(d,p) level. Transition state structure **M** is one way through which this pathway connects to pathway 2.

Barrier **M** to isomerization from **B** to **G** is 14.1 kcal/mol relative to **B**. The nitrogen to which hydrogen is bonded is nonplanar with a torsion angle of τ(N4−N2−O3−H1) = 122°. The features of this portion of the path suggest that the reactants might initially start out on one reaction path and move easily to the other through the isomerization from **B** to **G** (or vice versa) to continue on the other reaction path. Based upon the comparative heights of barriers **M** (13.4 kcal/mol) and **F** [the entrance channel barrier on path 2] (11.3 kcal/mol) relative to reactants, the formation of structure **G** is slightly favored energetically through traversing the entrance barrier **F**. However, under combustion conditions, the isomerization barrier **M** is also accessible, so path 2 could be reached by either TS **A** (via **M**) or **F**. Neither MMLM nor ref 7 reports this transition state **M**.

The TS most closely resembling **M** at the UMP2/6-311G-(d,p) level was given by ref 7 as a planar structure, labeled **6′**. The planarity of **6′** is in sharp contrast with the QCISD prediction of 109° for the torsion angle τ(ONNO). An attempt was made to locate this planar transition state **6′** using the basis set in the ref 7 study (i.e., 6-311G(d,p)) but at the QCISD level of correlation. Before the QCISD/6-311G(d,p) TS search was attempted, we reproduced planar structure **6′** from ref 7 through a transition-state optimization and subsequent normal-mode analysis at the MP2/6-311G(d,p) level. The MP2 geometry (which agreed with that published in ref 7) and corresponding force constant matrix (FCM) were used as the initial conditions for the QCISD/6-311G(d,p) TS search. The QCISD transition state search did not locate a cis planar saddle point, rather it found a cis planar minimum that is essentially identical to our minimum structure **B**. In Figure 4, the QCISD/6-311G(d,p) structures are compared with the purported MP2/6-311G(d,p) analogues from MMLM and ref 7. Table 3 contains the relative energies for these structures, and Table S2 in the Supporting Information reports their vibrational frequencies. Despite the larger basis set, all geometrical parameters from the QCISD/6-311G(d,p) calculations agree with the QCISD/6-31G(d,p) to within 1% for **B**. As a final attempt to locate **6′** at the QCISD/6-311G(d,p), the FCM was first calculated using the reported structure in ref 7. This FCM and the ref 7 structure were then used as the initial guess in a TS search which again converged on our local minimum **B**. We were unable to locate the ref 7 TS **6′** at the QCISD level. The near exact agreement between the QCISD predictions using the 6-31G(d,p) and 6-311G(d,p) basis sets suggests that the use of the smaller double-ζ basis adequately describes the valence space with respect to predicting reliable molecular structures for this system, at least for the minimum structures.

Returning to path 1 (shown in Figure 1), the reaction proceeds from **B** to **D** through a TS representing a 1,2-hydrogen shift to O3. This transition state is labeled **C** in Figure 1. The barrier to this hydrogen migration (51.2 kcal/mol) is the largest along this path. Therefore, this 1,2-hydrogen shift is the rate-determining step on path 1. The magnitude of this barrier precludes this reaction path as a contributor to thermal reaction under combustion conditions. While many steps were completed in the IRCs going from **C** toward **B** and **D**, none went to completion. The number of successful steps for each IRC is **C** → **B** (18); **C** → **D** (14). Optimizations were then performed using the geometries corresponding to the last successful IRC

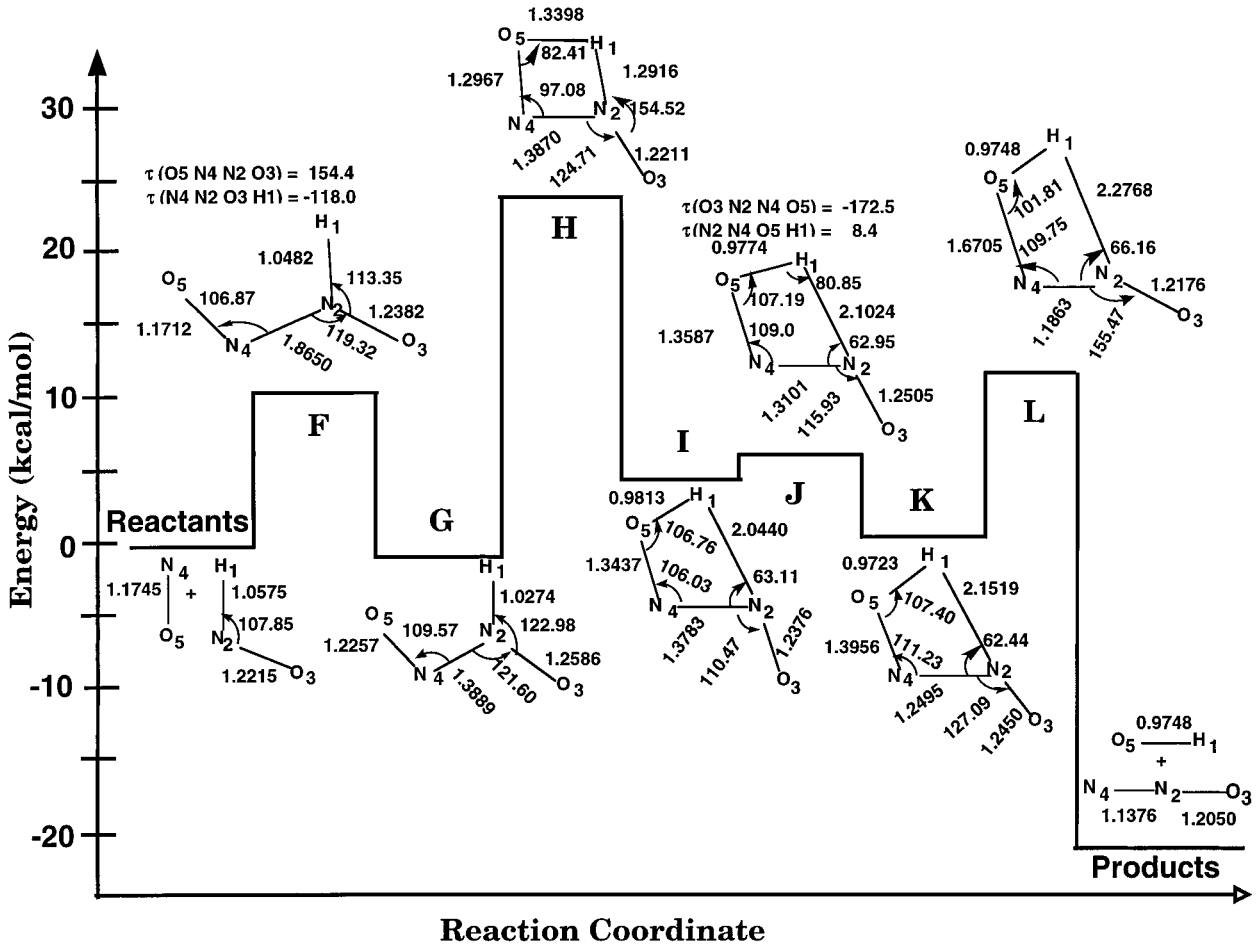

Figure 2. Pathway 2, reported here as the minimum energy reaction pathway, for reaction I. All structures and relative energies are for zero-point corrected energies calculated at the QCISD/6-311+G(2df,2p)//QCISD/6-31G(d,p) level.

step in each walk, and the resulting structures were consistent with **B** and **D**, respectively.

MMLM report a planar saddle point structure resembling our **C** (labeled **4″** in their paper) which also connects minima similar to **B** and **D** through a 1,2-hydrogen shift. They do not, however, report any nonplanar structure akin to our **C**. A TS search was initiated at the QCISD/6-31G(d,p) level to locate a planar analogue of **C**. Such a structure was located and is labeled **C′** in Figure 1. Vibrational analysis supports the assignment of this structure as a TS. Subsequent IRC calculations did not complete successfully, but ensuing optimizations connect this TS to **B** and **D**. The number of successfully converged steps along each IRC prior to optimization are **C′** → **B** (17); **C′** → **D** (18). The energy of **C** and **C′** relative to **B** are nearly identical, with **C′** lower than **C** by less than 1 kcal/mol.

To eliminate the possibility that our nonplanar **C** exists only as an artifact of the smaller basis set used in this study, **C** was again sought at the QCISD/6-311G(d,p) level starting with the QCISD/6-31G(d,p) optimized structure and force constant matrix. This converged on a **nonplanar** TS verified through vibrational analysis. The resulting structure had bond lengths which differed by 1% or less from the structure calculated with the double-ζ basis set, the simple angles differed by less than 0.6%, and the largest torsional difference was only 3°. Once again, the 6-31G(d,p) and 6-311G(d,p) calculations gave quantitatively similar structures at the QCISD level, this time for a TS.

Finally, a saddle point search was conducted to locate the planar **C′** structure at the QCISD/6-311G(d,p) level. This search converged, but the resulting vibrational analysis produced two imaginary eigenvalues, i.e., 2057i and 173i cm^{-1}. Repeated attempts to locate a true TS for the planar structure with the triple-ζ basis failed. These results cast doubt on the existence of the planar TS **C′**. It is also possible that a 1,3-hydrogen shift to O5 could occur, however no attempt was made to locate a saddle point for this type of hydrogen migration.

Once barrier **C** (or **C′**) is traversed, another intermediate is formed (structure **D**, Figure 1) in which the H−O bond distance is close to the asymptotic product value, the N−H separation is large at 1.87 Å, and the N−O is elongated to 1.42 Å. A final saddle point, **E**, leading to products has a structure in which both N−H and N−O distances are long (2.04 and 1.69 Å, respectively), indicative of the O−H separation from the N_2O moiety. Also, the NNO angle is approaching that of the linear conformation for the separated N_2O product. The magnitude of this barrier relative to the minimum for structure **D** is 4.6 kcal/mol. IRC calculations for the walk **E** → **D** proceeded until the local minimum corresponding to **D** was reached. The large energy release upon crossing barrier **C** (59 kcal/mol) and the small exit channel barrier **E** suggests that the intermediate **D** would be extremely short-lived. The IRC calculation for **E** → products was terminated when the energy was within 0.28 kcal/mol of the asymptote and the geometric parameters were within 0.3% or less of products.

B. Path 2. Path 2 is the MERP in this study, which can be compared with the MERP of MMLM as shown in Figure 3. The entrance channel transition state structure, **F** (see Figure 2), leading to formation of the HN(O)NO intermediate, is very similar to the entrance channel transition state for path 1 except for a trans structure in the heavy atoms. It is also a very loose

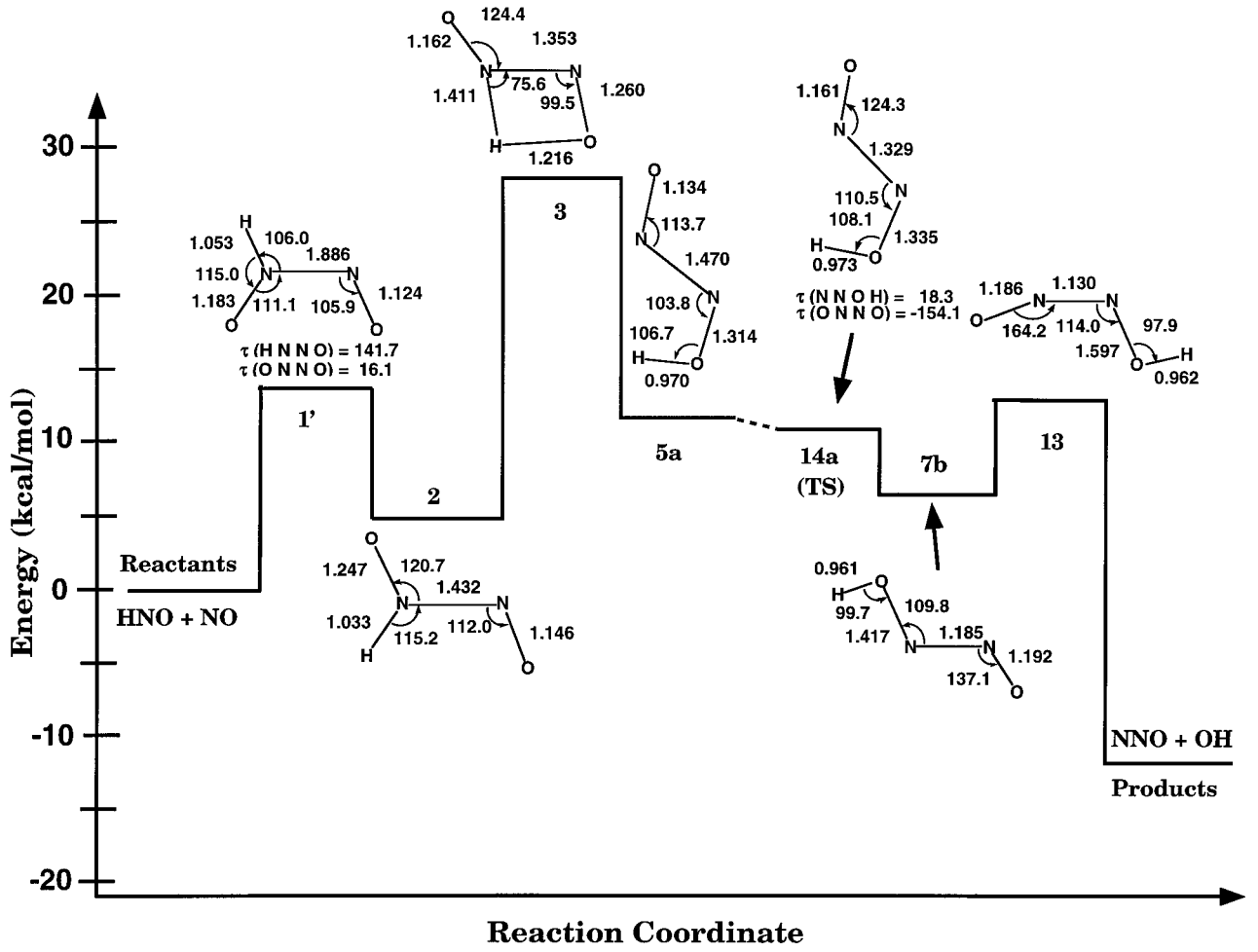

Figure 3. Reconstruction of MMLM's (ref 13) minimum energy reaction pathway for comparison with the current study's pathway 2. Energies taken from Figure 2 of ref 13 for values along the solid bold curve.

TS with a N−N separation of 1.86 Å. The barrier height is 11.3 kcal/mol, which is 2.9 kcal/mol higher than the analogous entrance channel barrier for path 1. The IRC walk toward reactants was halted after 46 steps. The structure at this point on the reaction path had an N−N separation of 2.84 Å, and the energy was within 0.4 kcal/mol of the isolated reactants. Also, all remaining structural parameters were within 0.2% of the reactants. Upon crossing this barrier, a minimum trans planar HN(O)NO intermediate, **G**, is formed that is similar to its cis planar counterpart in path 1. The IRC walk **F** → **G** aborted after 9 steps due to the updated Hessian having the "wrong number of negative eigenvalues". All of the bond lengths and angles agreed to within 0.2% of those in **G**, and the largest deviation between the two structures was a 3° difference in the ONNO dihedral angle. Also, the energy difference between this last point on the path and **G** was only 0.03 kcal/mol. Structure **G** is 0.3 kcal/mol lower in energy than its cis counterpart **B**. The reader is reminded that structure **G** connects to structure **B** on path 1 by the transition state **M**, as discussed in the preceding section.

The path leading from **F** to **G** represents the first of several differences in the connections along the MERP of this study and that of MMLM. MMLM report the entrance channel transition state to their MERP to be cis (structure **1′**), which then walks to a trans minimum, structure **2** (see Figure 3). The current study predicts a trans entrance channel TS (**F**) proceeding to a trans minimum structure **G** (see Figure 2). The nonplanar structure **F** of this study most closely resembles the MMLM planar TS structure **1**. For comparison, MMLM's structure **1** is reproduced in Figure 4 along with our structure **F**. The large N−N distance strongly suggests a very weak potential for rotation about the N−N bond, and hence no attempt was made to explore the issue of planarity in this conformer.

After crossing the entrance channel barrier, path 2 now proceeds through a 1,3-hydrogen shift to O5. The barrier (structure **H**, Figure 2) for the 1,3 shift is 24.0 kcal/mol relative to the reactants (25.0 kcal/mol relative to structure **G**). This barrier represents the rate-limiting step for this path, and its barrier height is close to the best predictions of MMLM (21.6 kcal/mol). Wilde[8] extracted an experimental estimate of 26 ± 5 kcal/mol for this barrier height from the data of Kaufman and Decker,[10] and Graven,[9] above 1000 °C. This experimental estimate is in good agreement with our value of 24.0 kcal/mol for **H**. The IRC for TS **H** toward **G** was terminated after 37 steps along the path. At this point, the energy was within 0.01 kcal/mol of that corresponding to structure **G**. All bond lengths and angles differed by no more than 0.2% from the optimized **G** structure, and torsion angles differed by less than 1°. The IRC from TS **H** toward products led to a local energy minimum, denoted as structure **I**. The IRC had proceeded to a structure whose energy was within 0.04 kcal/mol of the optimized structure **I**, and all structural parameters differed from those of structure **I** by less than 1%. **I** shows formation of the O−H bond concurrent with the breaking of the N−H bond. The H−O bond distance is close to the asymptotic product value, and the H−N separation is large at 2.04 Å.

Structure **I** resides in a very shallow well, from which the reaction proceeds over barrier **J**, which is 1.5 kcal/mol higher in energy. The most significant change in geometry as TS **J** is traversed is the opening of angle N4−N2−O3 as it approaches

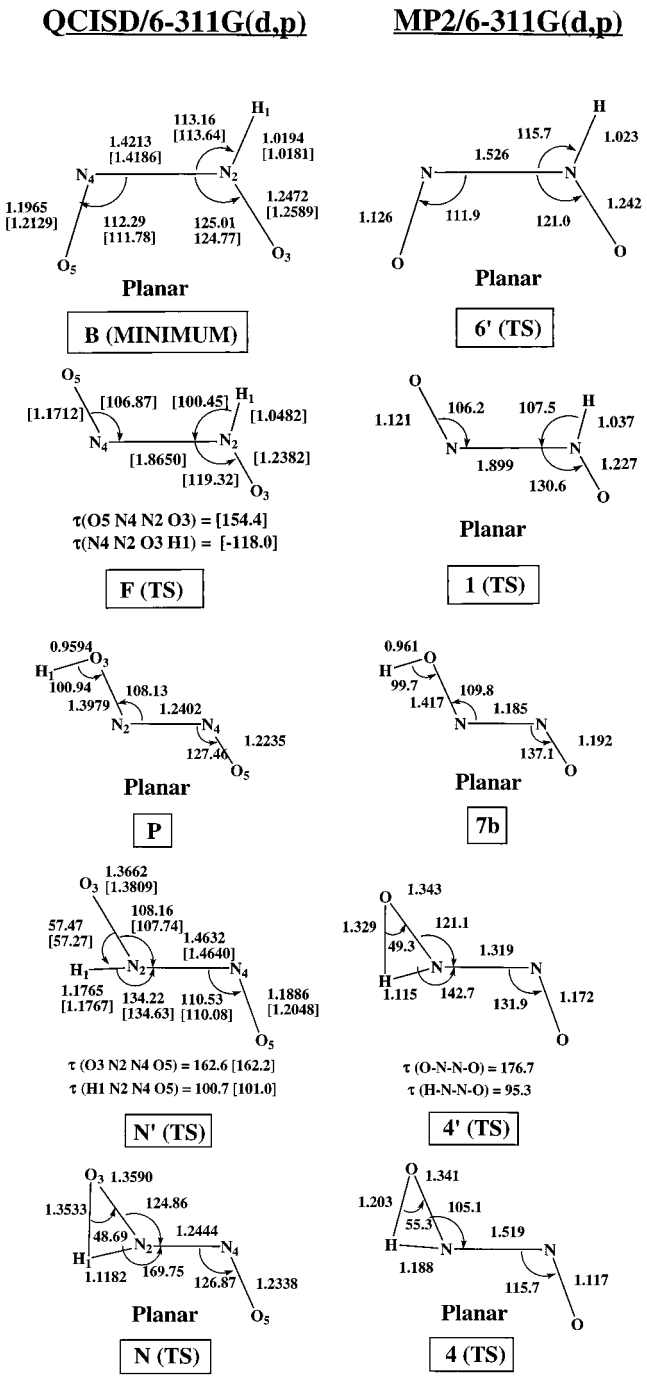

Figure 4. Comparison of structures calculated at the QCISD versus MP2 levels for the 6-311G(d,p) basis set. The MP2 structures **1**, **4**, **4′**, and **7b** are from MMLM (ref 13) and the MP2 structure **6′** from ref 7. The QCISD structures are from this study. Values in brackets are calculated using the 6-31G(d,p) basis set.

the linear conformation in the products. The N4−N2−O3 angle of the final intermediate, **K**, on path 2 has opened up to 127°. The final barrier **L** represents a simultaneous separation of the O−H group from the N_2O moiety and the further opening of the N_2O bond angle to 155° as it approaches the linear product. This final barrier is 11.3 kcal/mol relative to the minimum for structure **K**. The exit channel TS along MMLM's MERP is **13**. TS **13** (see Figure 3) corresponds to our TS structure **E** on path 1. MMLM report a second, higher energy exit channel TS labeled **12** (not shown in Figure 3), which has a cis ONNO arrangement, while TS **L** is trans. It is certainly possible that both **12** and **L** exist, and one connects to the other by a simple rotation about the N−N bond. The barrier to rotation is likely to be very small, and the molecule could easily pass from one structure to the other, so no attempt was made to locate TS **12**.

TABLE 3: Geometry Optimizations at QCISD/6-311G(d,p): Absolute Energies, Zero-Point Energies (ZPE), Zero-Point Corrected Relative Energies, and S^2 Values for Selected Species on the HNO + NO Potential Energy Surface

					QCISD/6-311G(d,p)	
species	type	S^2, 0[a]	S^2, A[b]	ZPE[c]	absolute E[d]	relative E[c,e]
HNO + NO	min	0.837	0.752	11.50	−259.832 023	
B	min	1.024	0.760	15.46	−259.829 193	5.74
C	TS	1.045	0.790	11.40	−259.737 071	59.48
C′	TS	1.021	0.785	2 imag. freqs	259.736 086	
N′	TS	1.078	0.791	11.31	−259.735 499	60.38
N	TS	1.217	0.790	11.71	−259.714 457	73.98
P(^{2}A′)[f]	min	1.122	0.773	15.70	−259.829 117	6.02

[a] The expectation value of S^2 before projection. [b] The expectation value of S^2 after projection. [c] Values given in kcal/mol. [d] Values given in hartrees. [e] Includes QCISD/6-311G(d,p) zero-point energy. [f] Symmetry of P within the C_S point group. See Table 1 for symmetry of other species in this table.

Further Comparisons with UMP2 Structures

C. J → K. Transition state structure **J** in the current study corresponds most closely to MMLM's structure **14a** in Figure 3. The torsion angle τ(H1−O5−N4−N2) for **J** is *cis*-, and the QCISD/6-31G(d,p) IRC walks from **J** to structure **K**, which is also cis. However, in MMLM's study the IRC from this transition state (structure **14a**) is reported to walk to a trans (H−O−N−N) planar structure (**7b**, Figure 3). To further explore this contrast between the two studies, we attempted to duplicate the calculations of MMLM by using the same correlation treatment (MP2) and basis set (6-311G(d,p)). Using the default tolerances for convergence criteria in the G92 set of programs, and beginning with MMLM's published structure and a MP2 FCM, we located the same transition state structure labeled **14a**. A frequency analysis verified it as a TS. Using the resulting FCM as input, an IRC calculation was performed in the direction of products. The walk would not converge due to apparent numerical problems. This was seen by the fact that after walking successfully for six optimized points along the IRC, the bond lengths for R(OH) and R(NN) went from the reasonable values of 0.97 and 1.21 Å, respectively, to the unrealistic values of 0.77 and 0.69 Å, respectively.

The calculations were repeated for the determination of the TS structure **14a**, followed by determination of the FCM for the optimized critical point. Both calculations used a tighter convergence criterion on the SCF density matrix. For the IRC calculations, Cartesian coordinates were used to follow the path (instead of the default mass-weighted internals), and the convergence tolerance on the SCF density matrix was set to "Converge=9" from the standard "Converge=8". This guarantees a RMS error in the density matrix of 1×10^{-9} or less, and an absolute error in the density matrix elements of 1×10^{-7} or less. The default settings were used for the accuracies of all other calculated properties. This IRC did indeed walk successfully to a converged structure (with default gradient convergence criteria), which corresponded to MMLM's cis planar structure **7a** (our structure **K**), not the trans planar structure **7b** reported by MMLM. There were no indications that any gradient step produced unrealistic structural parameters as in the previous run using the mass-weighted internal coordinates and default SCF convergence criterion. For the sake of completeness, the QCISD/6-311G(d,p) structure corresponding to MMLM's **7b** was located and is shown in Figure 4 as

structure **P**. Both geometries are planar, and the most notable quantitative difference is in the N−N−O angle, which differs by 10° between the MP2(137°) and QCISD(127°) values. These results seem to clearly demonstrate that MMLM's cis (H−O−N−N) transition state structure **14a** actually connects with the minimum intermediate **7a** at the MP2 level, which is also cis (H−O−N−N) planar, and not **7b** as previously reported. This corrected connection of cis (H−O−N−N) transition state with a cis (H−O−N−N) minimum structure at the MP2 level is now consistent with the QCISD/6-31G(d,p) results.

D. 1,2-Hydrogen Shifts. It is conceivable that products could be formed through a 1,2-hydrogen shift from trans structure **G** on path 2. This section will describe our attempts to locate transition states corresponding to such a mechanism. MMLM report two 1,2-hydrogen shift TS's corresponding to this reaction step; **4′** (nonplanar) and **4** (planar). These structures are illustrated in Figure 4 to facilitate comparison with the current results.

The nonplanar **4′** TS was sought at the QCISD/6-31G(d,p) level. The structure used as an initial guess corresponded to our structure **C**, except with a 180° rotation about the N−N bond. Structure **C** is the transition state for the 1,2-hydrogen shift from cis structure **B**. An SCF-level FCM corresponding to the initial structure was used as an initial guess. The results converged to a nonplanar structure denoted as **N′** in Figure 4. Structure **N′** has an energy of 60.38 kcal/mol (see Table 3) relative to reactants and was verified as a TS through vibrational analysis (see Table 2S in the Supporting Information). The QCISD structure has an N−N bond length that is 0.145 Å longer than that of structure **4′** reported by MMLM. Also, the QCISD O−N−N angles are considerably smaller than those of structure **4′** reported by MMLM. The QCISD structure has an O5−N4−N2 angle of 110°, which is smaller than the MMLM structure **4′** value by 22°. The QCISD/6-31G(d,p) structure **N′** more closely resembles the planar structure **4** reported by MMLM except for the nonplanarity of **N′**.

These structural differences could be due to differences in either the level of correlation or basis set. To test the basis set dependency, the transition-state search was rerun at the QCISD/6-311G(d,p) level, and the resulting converged transition state structure (confirmed through vibrational analysis) was almost identical with the structure determined using the smaller basis set (structure **N′**). The bond angles, bond lengths, and dihedral angles of the QCISD/6-311G(d,p) structure differed by 1% or less from **N′**. Structure **N′** represents the only geometry located in this study associated with **4′**, with rather poor agreement in angles between the two structures (see Figure 4).

MMLM's structure **4** was reproduced at the MP2/6-311G-(d,p) level and confirmed as a TS through vibrational analysis. A subsequent transition state search for structure **4** at the QCISD/6-311G(d,p) level was attempted using the MP2/6-311G(d,p) optimized structure for **4** and a QCISD/6-311G(d,p) FCM. The converged structure is a TS (see Table 2S in the Supporting Information), and is denoted as **N** in Figure 4. It is markedly different from MMLM's structure **4**, most notably in the N−N bond separation. The N−N bond distance in **N** is 1.244 Å, which is considerably shorter than the 1.519 Å of structure **4**. The ZPE-corrected energy of **N** relative to reactants is 73.98 kcal/mol (see Table 3). And once again, the two O−N−N angles for structure **N** deviate considerably from those of structure **4**. Finally, the structural dependence on basis set was tested by searching for structure **4** at the QCISD/6-31G-(d,f) level using the QCISD/6-311G(d,p) FCM and geometry as the initial guess. This calculation converged on a transition-state structure that was very similar to **N**. All QCISD/6-31G (d,p) structural parameters agree to within 1% or less of the QCISD/6-311G(d,p) values, once again demonstrating the suitability of the double-ζ basis set for structure determination.

The substantial dissimilarities between the MP2 and QCISD structures for **4** versus **N** and **4′** versus **N′** raise suspicions about the suitability of MP2 for predicting critical points on the PES for this system. From the standpoint of energetics, the QCISD/6-311G(d,p) barriers corresponding to the planar and nonplanar structures (**N** and **N′**, respectively) are 74 and 60 kcal/mol (Table 3) relative to reactants. Since these were so much higher in energy than the rate-limiting step on path 2, no further studies were conducted in search of a reaction path through the trans 1,2-hydrogen shift.

One structure on MMLM's MERP that has not yet been addressed by this study at the QCISD level is structure **7b**. It has been verified through an IRC walk that TS **N** connects to a minimum structure qualitatively similar to **7b** at the QCISD/6-311G(d,p) level. The IRC from **N** completed 17 steps, at which point an optimization was run that produced the minimum structure **P** in Figure 4. The relative energy of **P** is given in Table 3 as 6.02 kcal/mol, nearly identical to the relative energy of 6.1 kcal/mol for **7b** reported by MMLM. This route to forming **P** (MMLM's **7b**) via TS **N** does not preclude the possibility, in fact the likelihood, of forming **P** through the path predicted by MMLM, i.e, TS **14a** → **7b** (our **P**), which occurs by a rotation about the N−O bond in N−O−H (Figure 3). A comparison of **P** with **7b** shows that the most noteworthy structural difference between the QCISD and MP2 geometries is a 10° difference in the angle N2−N4−O5.

IV. Summary and Conclusions

We have presented results from an ab initio study of the reaction HNO + NO → HO + N_2O. Geometries of critical points were optimized at the QCISD/6-31G(d,p) level and characterized through normal-mode analyses. The results of this study provide two paths leading to formation of products through formation of various reaction intermediates. The reaction paths were established through IRC calculations leading from the transition states to connecting minima, which resulted in what appears to be the minimum energy reaction path (MERP) and a second, higher energy pathway. No claim is being made that these are the only pathways leading to products of reaction I. Rather, they constitute two completely connected pathways. The transition-state structure corresponding to the highest energy barrier on the MERP (denoted as **H**) in this study supports the conclusion of MMLM that their barrier structure **3** represents the rate determining step in the reaction HNO + NO → N_2O + OH. Establishment of this barrier height by MMLM is a very important result, since it is the first strong piece of evidence supporting the kinetic modelers' hypothesis that this reaction can play a major role in the gas-phase chemistry of burning nitramine propellants. MMLM also used QCISD, but only in determining the geometries of the reactants, products and TS **3.** Our best ZPE-corrected energy for this barrier height is 24 kcal/mol,to be compared with MMLM's "best" value of 21.6 kcal/mol, and the value 26 ± 5 kcal/mol extracted from experimental data.

Apart from agreeing on the rate-determining barrier, the current results differ most prominently from those of MMLM in the definition of the remaining MERP. In particular, our MERP entrance barrier has a trans (O−N−N−O) structure rather than the cis structure reported at the MP2 level by MMLM. Reaction proceeds through formation of a trans minimum intermediate **G** which then must overcome the rate-determining barrier **H**. Transition-state structure **H** is trans, in qualitative agreement with MMLM's MP2 structure **3**. After

crossing barrier **H**, the reaction proceeds to products while retaining the relative cis (H−O−N−N) and trans (O−N−N−O) torsional angle relationships seen in **H**. In contrast, MMLMs TS cis **14a** (our **J**) proceeds to a minimum intermediate which is trans (H−O−N−N) and then over their exit barrier **13** (which is still trans (H−O−N−N) to products. While their exit barrier **13** is lower than our cis (H−O−N−N) barrier, the IRC from our **J** (MMLM's **14a**) leads to a cis structure at both MP2 and QCISD, not the trans structure in MMLM. Almost certainly there exists a transition state (probably low-energy) leading from either **I** or **K** to such a *trans* (H−O−N−N) minimum intermediate like their **13**; however, it appears that **14a** is not the correct candidate. The current study predicts a MERP connection of

reactants → F → G → H → I → J → K → L → products

whereas MMLM predicts (using our nomenclature for structures)

reactants → A → G → H → I → J → P → E → products

Some of the QCISD structures are quantitatively and qualitatively dissimilar to the MP2 results of MMLM and ref 7. For example, the planar transition state **6′** (for rotation about the N−N bond) reported by ref 7 exists not as a TS, but as a minimum structure at the QCISD/6-311G(d,p) level. Its QCISD analogue in this study is the TS structure **M**, which is decidedly nonplanar. On the basis of its energy relative to reactants, **M** could most certainly be involved in the reaction dynamics that lead to products. Due to the expense of the QCISD/6-311G-(d,p) calculations, only a few other such comparisons for structures not on path 1 or path 2 were pursued, including the trans (O−N−N−O) 1,2-hydrogen shift TS structures **4** and **4′** of MMLM. The QCISD did indeed find analogues to these transition states, labeled **N** and **N′** in Figure 4. But the R(N−N) bond lengths differ between **4** and **N** by 0.28 Å, and one O−N−N angle by 20°. Similar disparities exist between the **4′** and **N′** geometries, where the R(N−N) differs by 0.14 Å and one O−N−N angle 21°. Fortunately, under combustion conditions **N′** and **N** are not likely to play a role in the reaction leading to products. Neither MMLM nor ref 7 reports a transition state structure analogous to our exit barrier **L**, a structure with cis (HONN) and trans (ONNO). One last notable difference between our QCISD/6-31G(d,p) calculations and the MP2 results reported by ref 7 is for our cis planar structure **B**. Reference 7 reports a cis planar structure, labeled **6′**, which is similar to our minimum structure **B**, but they report that it "...corresponds to the transition state for the internal rotation around the N−N bond." However, our structure **B** is a minimum, not a transition state. These predicted differences in structures between QCISD and MP2, some of which are quite large, could produce subsequently large errors in the relative energetics, vibrational frequencies, and normal modes of the species on the PES. This, coupled with the differences in connectivity predicted by the IRC walks could play a major role in the outcome of a dynamical simulation for reaction I.

Acknowledgment. A significant portion of these calculations were performed on the Silicon Graphics Incorporated Power Challenge Array located at the DOD High Performance Computing site, U.S. Army Research Laboratory, Aberdeen, Maryland.

Supporting Information Available: Vibrational frequencies are given for structures in Table 1 calculated at the QCISD/6-31G(d,p) level and for structures in Table 3 calculated at the QCISD/6-311G(d,p) level (2 pages). Ordering information is given on any current masthead page.

References and Notes

(1) Vanderhoff, J. A.; Anderson, W. A.; Kotlar, A. J. *Proceedings 29th JANNAF Combustion Meeting*, CPIA Publication 593, 1992; *II*, p 225.
(2) Diau, E. W. G.; Lin, M. C.; He, Y.; Melius, C. F. *Prog. Energy Combust. Sci.* **1995**, *21*, 1.
(3) Diau, E. W. G.; Halbgewachs, M. J.; Smith, A. R.; Lin, M. C. *Int. J. Chem. Kinet.* **1995**, *27*, 867.
(4) Soto, M. R.; Page, M. *J. Chem. Phys.* **1992**, *97*, 7287.
(5) Soto, M. R.; Page, M.; McKee, M. L. *Chem. Phys.* **1991**, *153*, 415.
(6) Soto, M. R.; Page, M.; McKee, M. L. *Chem. Phys. Lett.* **1991**, *187*, 335.
(7) Mebel, A. M.; Morokuma, K.; Lin, M. C. *J. Chem. Phys.* **1994**, *101*, 3916.
(8) Wilde, K. A. *Combust. Flame* **1969**, *13*, 173.
(9) Graven, W. M. *J. Am. Chem. Soc.* **1957**, *79*, 3657.
(10) Kaufman, F.; Decker, L. J. *Symp. Int. Combust. Proc.* **1959**, *8*, 139.
(11) Hinschelwood, C. N.; Green, T. E. *J. Chem. Soc.* **1926**, 730.
(12) Hinschelwood, C. N.; Mitchell, J. W. *J. Chem. Soc.* **1936**, 378.
(13) Mebel, A. M.; Morokuma, K.; Lin, M. C.; Melius, C. F. *J. Phys. Chem.* **1995**, *99*, 1900.
(14) (a) Pople, J. A.; Head-Gordon, M.; Fox, D. J.; Raghavachari, K.; Curtiss, L. A. *J. Chem. Phys.* **1989** *90*, 5622. (b) Curtiss, L. A.; Jones, C.; Trucks, G. W.; Ragavachari, K.; Pople, J. A. *J. Chem. Phys.* **1990**, *93*, 2537. (c) Curtiss, L. A.; Raghavachari, K.; Trucks, G. W.; Pople, J. A. *J. Chem. Phys.* **1991**, *94*, 7221.
(15) Moeller, C.; Plesset, M. S. *Phys. Rev.* **1934**, *46*, 618.
(16) Nobes, R. H.; Moncrieff, D.; Wong, M. U.; Radom, L. *Chem. Phys. Lett.* **1991**, *182*, 216.
(17) Handy, N. C.; Knowles, P. J.; Somasundram, K. *Theor. Chim. Acta* **1985**, *68*, 87.
(18) Chen, Y.; Schlegel, H. B. *J. Chem. Phys.* **1994**, *101*, 5957.
(19) Ma, N. L.; Smith, B. J.; Radom, L. *Chem. Phys. Lett.* **1992**, *193*, 386.
(20) Stanton, J. F. *J. Chem. Phys.* **1994**, *101*, 371.
(21) Rice, B. M.; Chabalowski, C. F. *J. Phys. Chem.* **1994**, *98*, 9488.
(22) Lee, T. J.; Rendell, A. P.; Taylor, P. R.; *J. Phys. Chem.* **1990**, *94*, 5463.
(23) Pople, J. A.; Head-Gordon, M.; Raghavachari, K. *J. Chem. Phys.* **1987**, *87*, 5968. Salter, E. A.; Trucks, G. W.; Bartlett, R. J. *J. Chem. Phys.* **1989**, *90*, 1752. Foresman, J. B.; Head-Gordon, M.; Pople, J. A.; Frisch, M. J. *J. Phys. Chem.* **1992**, *96*, 135.
(24) Hehre, W. J.; Ditchfield, R.; Pople, J. A. *J. Chem. Phys.* **1972,** *56*, 2257. Hariharan, P. C.; Pople, J. A. *Theor. Chim. Acta* **1973**, *28*, 213.
(25) Seeger, R.; Pople, J. A., *J. Chem. Phys.* **1977**, *66*, 3045.
(26) (a) Gonzalez, C.; Schlegel, H. B., J. Chem. Phys. **1989**, *90*, 2154. (b) Gonzalez, C.; Schlegel, H. B. *J. Phys. Chem.* **1990**, *94*, 5523.
(27) Krishnan, R.; Binkley, J. S.; Seeger, R.; Pople, J. A. *J. Chem. Phys.* **1980**, *72*, 650. McLean, A. D.; Chandler, G. S. *J. Chem. Phys.* **1980**, *72*, 5639.
(28) Clark, T.; Chandrasekhar, J.; Spitznagel, G. W.; Schleyer, P. v. R. *J. Comput. Chem.* **1983**, *4*, 294.
(29) Frisch, M. J.; Pople, J. A.; Binkley, J. S. *J. Chem. Phys.* **1984**, *80*, 3265.
(30) (a) Frisch, M. J.; Trucks, G. W.; Head-Gordon, M.; Gill, F. M. W.; Wong, M. W.; Foresman, J. B.; Johnson, B. G.; Schlegel, H. B.; Robb, M. A.; Replogle, E. S.; Gomperts, R.; Andres, J. L.; Raghavachari, K.; Binkley, J. S.; Gonzalez, C.; Martin, R. L.; Fox, D. J.; Defrees, D. J.; Baker, J.; Stewart J. J. P.; Pople, J. A. *Gaussian 92, Revision A*; Gaussian, Inc.: Pittsburgh, PA, 1992. (b) Frisch, M. J.; Trucks, G. W.; Schlegel, H. B.; Gill, P. M. W.; Johnson, B. G.; Robb, M. A.; Cheeseman, J. R.; Keith, T.; Petersson, G. A.; Montgomery, J. A.; Raghavachari, K.; Al-Laham, M. A.; Zakrzewski, V. G.; Ortiz, J. V.; Foresman, J. B.; Cioslowski, J.; Stefanov, B. B.; Nanayakkara, A.; Challacombe, M.; Peng, C. Y.; Ayala, P. Y.; Chen, W.; Wong, M. W.; Andres, J. L.; Replogle, E. S.; Gomperts, R.; Martin, R. L.; Fox, D. J.; Binkley, J. S.; Defrees, D. J.; Baker, J.; Stewart, J. P.; Head-Gordon, M.; Gonzalez, C.; Pople, J. A. *Gaussian 94, Revision B.1*; Gaussian, Inc.: Pittsburgh PA, 1995.
(31) Cizek, J. *Adv. Chem. Phys.* **1969**, *14*, 35.
(32) Purvis, G. D.; Bartlett, R. *J. Chem. Phys.* **1982**, *76*, 1910.
(33) Scuseria, G. E.; Schaefer, H. F. *J. Chem. Phys.* **1989**, *90*, 3700.
(34) (a) ACES II is an ab initio program system written by J. F. Stanton, J. Gauss, J. D. Watts, W. J. Lauderdale, and R. J. Bartlett. It includes the VMOL and VPROPS integral packages of J. Almlof and P. R. Taylor and the ABACUS integral derivative package of T. Helgaker, H. J. Aa. Jensen, P. Jorgensen, J. Olsen, and P. R. Taylor. (b) Stanton, J. F.; Gauss, J.; Watts, J. D.; Lauderdale, W. J.; Bartlett, R. J. *Int. J. Quantum Chem. Symp.* **1992**, *26*, 879.
(35) Paldus, J.; Cizek, J.; Jeziorski, B. *J. Chem. Phys.* **1989**, *90*, 4356.
(36) Pople, J. A.; Head-Gordon, M.; Raghavachari, K. *J. Chem. Phys.* **1989**, *90*, 4635.
(37) Bartlett, R. J. *J. Phys. Chem.* **1989**, *93*, 1697.